Author(s): Juarez Mosqueda, Rosalba; Kaappa, Sami; Malola, Sami; Häkkinen, Hannu

Title: Analysis of the Electronic Structure of Non-Spherical Ligand-Protected Metal Nanoclusters : The Case of a Box-Like Ag67

Year: 2017

Version:

Please cite the original version:

Juarez Mosqueda, R., Kaappa, S., Malola, S., & Häkkinen, H. (2017). Analysis of the Electronic Structure of Non-Spherical Ligand-Protected Metal Nanoclusters : The Case of a Box-Like Ag67. Journal of Physical Chemistry C, 121(20), 10698-10705. https://doi.org/10.1021/acs.jpcc.6b10618

Analysis of the Electronic Structure of Non-Spherical Ligand-Protected Metal Nanoclusters: The Case of a Box-Like Ag_{67}

Rosalba Juarez-Mosqueda,[†§] Sami Kaappa,[†§] Sami Malola,[†] Hannu Häkkinen[†‡]*

[†]Department of Physics and [‡]Department of Chemistry, Nanoscience Center, University of Jyväskylä, FI-40014 Jyväskylä, Finland

ABSTRACT: In this work we introduce a new strategy to investigate the electronic shell structure of ligand-protected metal nanoclusters of polyhedral core shape. The central idea is to identify the symmetry of the Kohn-Sham molecular orbitals of an atomistic structure based on their projection onto the electronic states of a jellium system with a similar shape of the background charge density. Herein, we study the connection between a reduced atomistic model of the recently reported box-like $[Ag_{67}(SR)_{32}(PR_3)_8]^{3+}$ nanocluster and a jellium box consisting of 32 free electrons. With this approach, we determine the symmetry of electronic states of the metal core and identify those that are involved in the lowest metal-to-metal electronic transitions. Furthermore, we define a new transition selection rule for ligand-protected metal nanoclusters with rectangular cuboid-like core. This rule differs from the one of a particle in an infinitely deep 3D potential well. The approach presented here is complementary to the angular momentum analysis of "superatom orbitals" of spherical or near spherical metal nanoclusters and opens the

door to understand and predict the electronic properties and stability of several existent and new ligand-protected metal nanoclusters with non-spherical cores.

INTRODUCTION

Valence electrons of small 1-2 nm sized metal nanoclusters consisting of less than a few hundred atoms are often delocalized over the full cluster volume, leading to quantized valence electron states.[1–4] The size and the shape of the confinement strongly affect the energies and symmetries of these states. Occupying the states by the Pauli principle gives a sequence of electron-shell-closing numbers, which for spherical or near-spherical systems resemble closely to shell-filling numbers of ordinary atoms. Hence the terms of “artificial atom” or “superatom” have been used in the context of cluster physics already for a long time.[1–5] Despite the stability factors, the low coordinated atoms at the surface of small nanoclusters tend to react with foreign atoms and molecules especially in non-closed shell nanoclusters.[6–8] Less reactive surfaces can be achieved with ligated metal nanoparticles that all have a common structure of a metallic core overlaid by organic molecules such as thiols, phosphines, and alkynyls. Synthesis of the ligated metal nanoclusters can be made with molecular precision and the choice of ligands affects their overall structure, size and physical, chemical, and biological properties.[9–16] As a consequence of the stabilizing factors from the metal-ligand interface, ligand-protected metal nanoclusters can be very stable also in non-spherical shapes.[17–20] Developments in synthesis of stable non-spherical shaped nanoclusters extend the already vast variety of intriguing properties of these systems to be used in different applications.

Häkkinen and collaborators[21,22] laid out two principles concerning both the geometric and electronic structure of ligand-protected metal nanoclusters in 2006-2008. First, the atomic

structure of theses clusters can generally be understood by the "Divide and Protect" concept, whereby the metal atoms (*M*) could be found in the cluster in two chemical (formal oxidation) states, in the neutral state in the central metal core and in +1 state if bound to electron-withdrawing ligands (*X*) inside the ligand layer.[21] Second, as the chemical formula of these clusters can be written in a simplest form as $(M_mX_xL_s)^q$ where additionally *L* denotes a weakly (coordinating) bound ligand and *q* a possible overall charge of the cluster, the number of the "metallic" ("free") electrons *n* in the system can be calculated simply from the equation

$$n = m - x - q$$

when *M* is assumed to be a monovalent metal and *X* a one-electron withdrawing ligand.[22] Generalisation of the equation to multivalent metals and ligands is straightforward.

The number of electron withdrawing ligands and the number of valence electrons of metal atoms in the nanocluster determine thus the electronic structure which includes, among all, the superatomic orbitals delocalized over the metallic core. For the spherical nanoclusters, electronic shells close when the free valence electrons of the superatom system equals to magic numbers 2, 8, 18, 34, 58, 92, 138,... indicating increased electronic stability. For a spherical ligand-protected nanocluster the projection of the electron states onto spherical harmonics directly reveals their superatomic nature.[22] Up to date, the applicability of this approach has been restricted to spherical symmetry, hence to spherical and close-to-spherical nanoclusters.

Recently, several ligand-protected metal nanoclusters have been reported which are far from spherical shape.[17–20] As an example, Alhilaly *et. al.*[17] synthesized an unprecedented box-like shaped silver nanocluster formed by 67 Ag atoms (Ag_{67}) protected by thiol and phosphine ligands. This new nanocluster, formulated as $[Ag_{67}(SPhMe_2)_{32}(PPh_3)_8]^{3+}$, has been fully characterized by X-ray diffraction and electrospray ionization mass spectrometry (ESI-MS). The

authors attribute the shape and stability of the cluster partly to the thiols, but most importantly to the phosphine ligands at each corner of the box. They also reported the optical spectrum of this $[Ag_{67}(SPhMe_2)_{32}(PPh_3)_8]^{3+}$ compound which shows highly structured absorption peaks in the visible region. Their results underline the importance of the protecting ligands in determining the shape and size of the cluster core.

In this work, we extend the analysis of electronic shells of spherical superatoms to non-spherical shapes. The idea is based on the projection of the molecular orbitals of the atomistic cluster onto quantum states of a jellium system with similar background charge density as in the metal core of the real system. Using this approach we analyze the symmetries of the electronic states for the box-like $[Ag_{67}(SPhMe_2)_{32}(PPh_3)_8]^{3+}$ nanocluster[17] using a simplified $[Ag_{67}(SH)_{32}(PH_3)_8]^{3+}$ model. Moreover, we analyze the electronic transitions related to the absorption peaks of the highly structured optical spectrum and obtain a new transition selection rule for ligand protected metal nanoclusters with rectangular cuboid-like core. In contrast to the transition selection rule for a particle in a 3D infinite potential well, this new rule considers the effect of the electron-electron interactions and the finite potential well of the real nanoclusters.

COMPUTATIONAL METHODS

The electronic structure calculations of both the atomistic $[Ag_{67}(SH)_{32}(PH_3)_8]^{3+}$ and the jellium models were performed using the projector augmented-wave (PAW) method as implemented in the GPAW code-package (grid-based projector-augmented wave method).[23,24] The wave functions were represented by using a real-space with grid spacing of 0.2 Å. The coordinates of the atomistic model were built from the experimental $[Ag_{67}(SPhMe_2)_{32}(PPh_3)_8]^{3+}$ crystal structure[17] by replacing the true ligands with the -SH and -PH_3 groups. All the atomic positions

in the $[Ag_{67}(SH)_{32}(PH_3)_8]^{3+}$ model were optimized using the convergence criterion of 0.05 eV/Å as a maximum value for the forces acting on individual atoms.

Based on the electron count formula for ligand protected nanoclusters[22] the $[Ag_{67}(SR)_{32}(PR_3)_8]^{3+}$ system consists of 32 superatom electrons (n = 67 – 32 – (+3) = 32), since the phosphine ligands do not withdraw or donate electrons to the system. The jellium model was therefore designed as 32 electrons confined in an ion density box of the same shape and dimensions as the metal core of the atomistic model (see **Figure 1**). To take the effect of the ligand layer into account in the jellium model, an ion charge of +44e was used to yield an effective charge of +12e (+44e – 32e = +12e, e stands for the positive unit charge). The value +12e was obtained from the Bader charge analysis[25] by taking the sum of the atomic charges of the sixty-seven silver atoms in the $[Ag_{67}(SH)_{32}(PH_3)_8]^{3+}$ cluster.

The ground state calculations for the $[Ag_{67}(SH)_{32}(PH_3)_8]^{3+}$ and jellium models were performed using the Kohn-Sham formulation of the density functional theory (DFT) as implemented in GPAW. The exchange and correlation energy for the atomistic calculations was approximated by using the generalized gradient-corrected PBE[26] functional. The jellium calculations were performed using local-density approximation (LDA)[27] that, in contracts to the PBE functional, neglects the gradient of the electron density. Nevertheless, this effect is very small in jellium calculations since the gradients are relatively small.

To identify symmetry of the electronic states, the Kohn-Sham molecular orbitals of the atomistic model were projected onto the jellium states and the overlaps were calculated through the integrals $\mathcal{O}_{ij} = \int \phi_i(\vec{r})\psi_j(\vec{r})d\vec{r}$, where $\psi_j(\vec{r})$ and $\phi_i(\vec{r})$are the sets of wave functions from the atomistic and jellium calculations, respectively (see more details in Supporting Information SI). The square of the overlap between $\psi_j(\vec{r})$ and $\phi_i(\vec{r})$ was used as a quantitative measure in

characterizing the symmetry of the atomic state. The nodal multiplicities in the jellium model were defined by visual inspection as (n_x ,n_y, n_z) where n_x, n_y, and n_z indicate the number of nodes along the *x*, *y* and *z* dimensions of the models shown in **Figure 1**.

The linear response time-dependent density functional theory (LR-TDDFT) was used to calculate the optical spectrum and the oscillator strengths of the individual transitions.[28,29] The electronic transitions were analyzed using the transition contribution maps (TCMs) based on the time-dependent density functional perturbation theory (TD-DFPT)[30,31] by using the photon with the same energy as the absorption peak of interest and a dipole moment μ directed either along the longest dimension (*z*) of the metal core or along one of the shorter ones (*y*) (see **Figure 1**). All the excited state calculations were performed using the PBE functional.

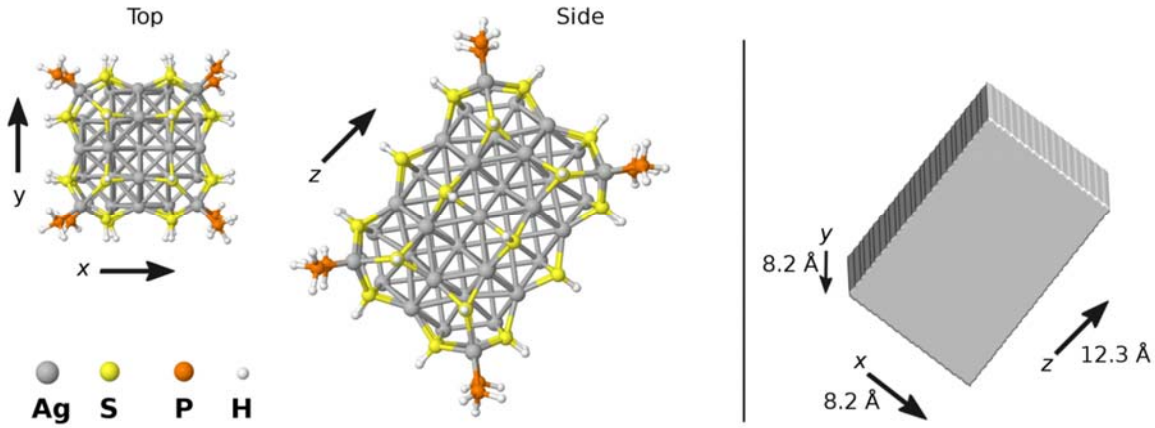

Figure 1. (Left) top and side views of the atomistic $[Ag_{67}(SH)_{32}(PH_3)_8]^{3+}$ model. (Right) shape of the background density of the jellium model consisting of 32 electrons and a net charge of +12*e*. The dimensions of the jellium system correspond to the dimensions of the silver core in the atomistic model.

RESULTS AND DISCUSSION

In the optimized $[Ag_{67}(SH)_{32}(PH_3)_8]^{3+}$ nanocluster, the Ag-Ag bond distances are ~1% larger than the ones from the experimental structure. The S-Ag and P-Ag bonds however retained the same lengths (2.5 Å and 2.4 Å, respectively) as in the crystal structure. The comparison between the experimental and the calculated optical spectra shown in **Figure 2**, reveals that removing the phenyl ligands does not modify the main spectral features within the range of 650 – 1100 nm, but it significantly changes the spectrum at higher energy region. Moreover, the lack of the true ligands produces a blue-shifting of the spectrum by 87 nm as a consequence of the confinement of the electron density within the boundaries of the metal core. This was already reported in the paper of Alhilaly *et al.*[17]

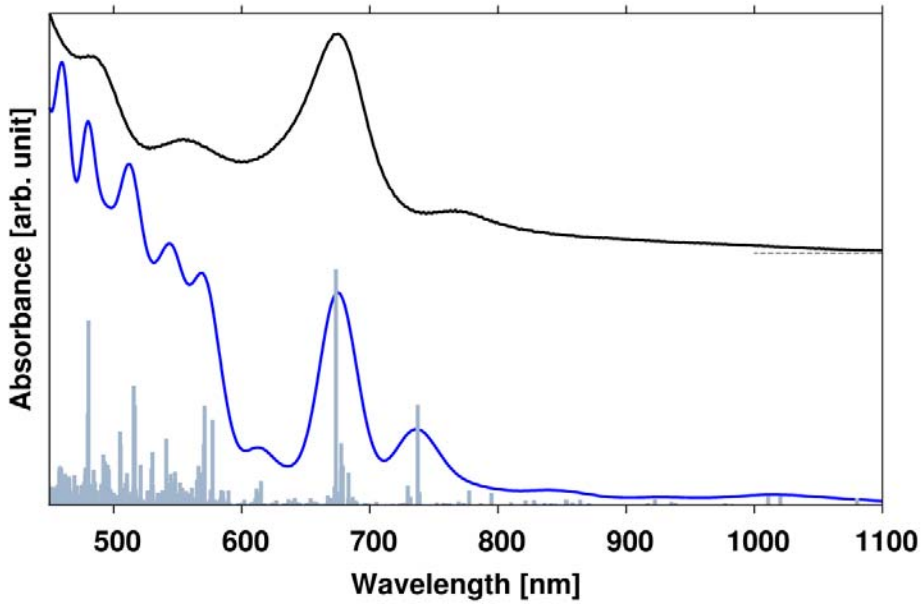

Figure 2. (black) experimental absorption spectrum of the $[Ag_{67}(SPhMe_2)_{32}(PPh_3)_8]^{3+}$ nanocluster, and (blue) the calculated spectrum of the $[Ag_{67}(SH)_{32}(PH_3)_8]^{3+}$ model. (Gray) the oscillator strength of individual transitions is plotted as delta-function-like peaks. The calculated spectrum is the sum of

Gaussian smoothed individual transitions (width of 0.05 eV). The oscillator strengths and calculated spectrum are red-shifted by 87 nm to compare the main spectral features with the experimental data.

To understand the nature of the molecular orbitals delocalized inside the metal core and to identify those that are involved in the electronic transitions with high oscillator strengths, we analyzed the symmetry of the electronic states formed in a jellium system of same charge density, shape, and size as in the metal core of the $[Ag_{67}(SH)_{32}(PH_3)_8]^{3+}$ nanocluster. The symmetry of the jellium states was determined by the number of nodes along the *x*, *y* and *z* dimensions of the jellium model. The total number of nodes is given then by the sum of the nodal multiplicities as $n_x + n_y + n_z$. The projection of the Kohn-Sham molecular orbitals of the $[Ag_{67}(SH)_{32}(PH_3)_8]^{3+}$ nanocluster onto the "clean" jellium states allowed us to identify the symmetry of the metal core states. This new method is comparable to the known approach of projecting the wave functions to spherical harmonics but allows studying also non-spherical nanoclusters. The assignment of the state symmetries is based on the weights given by the overlap integrals as described in the SI text. In **Figure 3** we depict the shape and indicate the symmetry of nine occupied molecular orbitals (HOMO to HOMO-8, and HOMO-446), and fifteen unoccupied ones (LUMO to LUMO+13, and LUMO+17). The values (between 0 and 1) above the arrows correspond to the highest weights found from the square of the overlap integrals. Remembering that the overlap integrals were calculated for whole nanocluster including the ligand layer, the values between 0.19-0.67 in Fig. 3 indicate a good correspondence between the symmetries of the jellium state and the corresponding molecular orbital of the $[Ag_{67}(SH)_{32}(PH_3)_8]^{3+}$ nanocluster. In comparison, the states located between -1.0 eV and -2.25 eV show very low overlap values (below 0.08) to any of the jellium states. Therefore these states

are assigned as ligand states (LS). Exceptional case is observed for the molecular orbitals at -0.84 eV and -0.83 eV whose symmetry is uncertain. These two states together resemble the jellium state with nodal multiplicities (1,1,1), which seems to get split in the atomistic system.

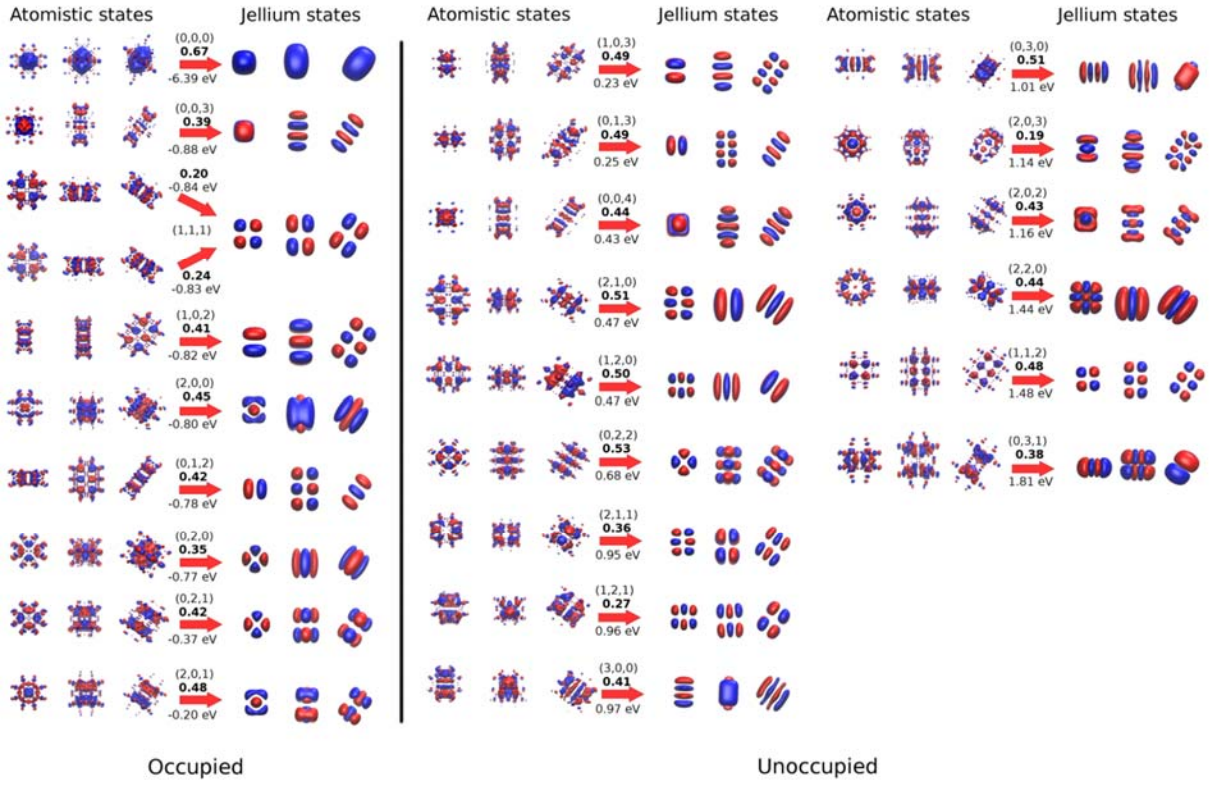

Figure 3. (Left) occupied and (right) unoccupied Kohn-Sham states of the atomistic $[Ag_{67}(SH)_{32}(PH_3)_8]^{3+}$ and jellium models located close to the HOMO-LUMO region. The energy and nodal multiplicities (n_x, n_y, n_z) of the states are indicated below and above the arrows. The weights of the overlap between the molecular orbitals and the jellium quantum states are indicated in bold letters above the arrow. The states with (2,0,1) and (1,0,3) symmetry are the HOMO and LUMO, respectively. The most spherical state with no nodes (0,0,0) is located 6.39 eV below the Fermi level (first in the list on the left).

The weights from overlap integrals were broadened (with a Gaussian function of width = 0.01 eV) and plotted as projected local density of states (PLDOS) for sets of electronic states with the same number of total nodes. The PLDOS and TCMs are plotted together in **Figure 4** to gain insight into the metal-to-metal electronic transitions analyzed for the spectral peaks at 587 nm (2.11 eV) and 648 nm (1.91 eV). The excitation profiles were analyzed along the *y*- and *z*-dimensions of the atomistic model by using a laser field with dipole moment μ_y and μ_z in each respective case. The transitions are labeled with the letters A–N in the TCMs.

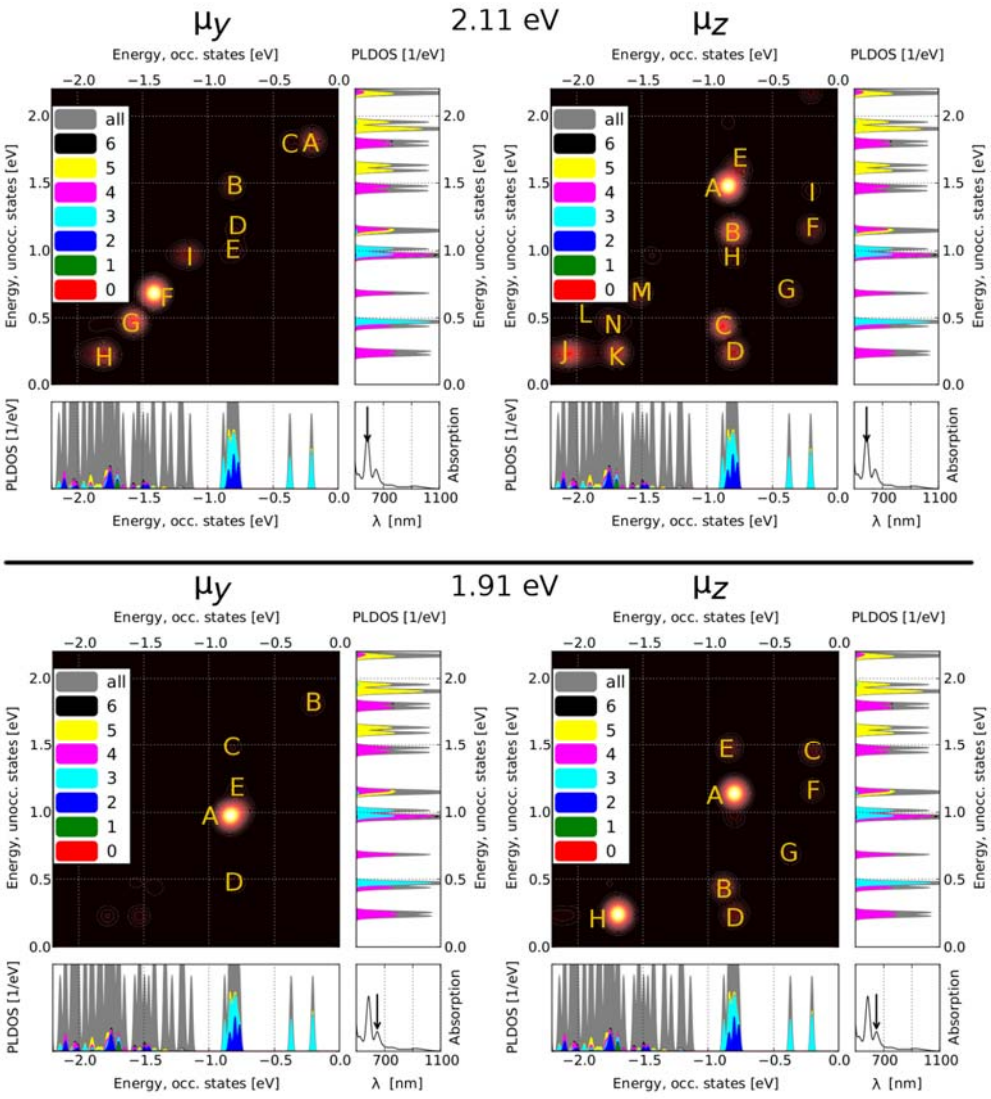

Figure 4. Transition contribution maps (TCMs) for the spectral features of the $[Ag_{67}(SH)_{32}(PH_3)_8]^{3+}$ cluster. The electronic transitions are analyzed by using photon energy of 2.11 eV (top) and 1.91 eV (bottom) and dipole moment μ directed either along the *y*- (μ_y) or *z*- (μ_z) dimension of metal core. The bright spots labeled with the letters A-N highlight the strongest contributions. The PLDOS based on the overlap between the jellium states and the molecular orbitals of the $[Ag_{67}(SH)_{32}(PH_3)_8]^{3+}$ cluster are plotted below (occupied) and next to (unoccupied) the TCM. The colors indicate the total number of nodes. Gray shows the total density of states of the cluster. The arrow in the optical spectrum (bottom-right) points to the analyzed absorption peak. Note that the optical spectra shown in the bottom right part of each panel does not include the red-shift used in Figure 2.

The relative intensities of the electronic transitions (calculated with respect to the total intensity) are shown in percentages in **Table 1**. The results indicate that at 587 nm (2.11 eV), the most intense metal-to-metal electronic transitions (with relative intensity >7%) occurring along the *y* dimension involve the states with nodal multiplicities (2,0,1) → (0,3,1), and (0,2,1) → (0,3,1). Using the same photon energy but a dipole moment oriented along the *z* dimension of the metal core, the strongest transitions are between the states with symmetries (1,1,1) → (1,1,2), (2,0,0) → (2,0,3), and (0,0,3) → (0,0,4). Similarly, for the absorption peak at 648 nm (1.91 eV) the transitions in the metal core along the *y* dimension involve the states with nodal multiplicities (1,1,1) → (3,0,0), (0,2,0) → (0,3,0), and (1,1,1) → (1,2,1), and along the *z* dimension the transitions are between the states with symmetries (2,0,0) → (2,0,3) (see **Table 1**). The electronic transitions for the spectral peaks at 751 nm (1.65 eV) and 928 nm (1.33 eV) are also analyzed and the results are provided in the **SI** (see **Figure S1 and Table S1**).

Table 1. Nodal multiplicities (n_x, n_y, n_z) of the Kohn-Sham molecular orbitals of the $[Ag_{67}(SH)_{32}(PH_3)_8]^{3+}$ nanocluster involved in the most intense electronic transitions. The transitions are analyzed for the absorption spectral peaks at 587 nm (2.11 eV) and 648 nm (1.91 eV) by using a laser field with the same photon energy and a dipole moment (μ) directed towards either the *y* (μ_y) or the *z* (μ_z) dimension. The letters from A-N refer to the bright spots shown in the TCMs. The values in the square brackets show the relative intensity (in percentage) of the transitions with respect to the total intensity. LS is used to indicate "ligand states".

Energy of the transition	Direction of the μ	A	B	C	D	E	F	G	H	I	J,K	L,M	N
	y	(2,0,1)→(0,3,1) [7.5%] (0,2,1)→(0,3,1) [7.5%]	(1,0,2)→(1,1,2) [3.2%]	(0,2,1)→(0,3,1) [1.4%]	(0,1,2)→ (2,0,2) [1.3%]	(0,2,0)→(0,3,0) [0.7%] (1,1,1)→(3,0,0) [0.3%] (2,0,0)→(0,3,0) [0.3%]	LS→(0,2,2) [42%]	LS→(1,2,0) [17%] LS→(0,0,4) [0.3%]	LS→(1,0,3) [11%] LS→(0,1,3) [0.3%]	LS→(1,2,1) [5.3%] LS→(3,0,0) [0.9%]	-	-	-
	z	(1,1,1)→(1,1,2) [23.9%]	(2,0,0)→(2,0,3) [9.9%]	(0,0,3)→(0,0,4) [8.9%]	(0,1,2)→(0,1,3) [3.2%] (1,0,2)→(1,0,3) [3.0%]	(0,2,0)→(0,2,3) [2.9%]	(2,0,1)→(2,0,2) [2.6%]	(0,2,1)→(0,2,2) [1.7%]	(0,1,2)→(2,1,1) [0.7%]	(2,0,1)→(2,2,0) [1.1%]	LS→(1,0,3) [8.3%] and [2.0%] LS→(0,1,3) [2.7%] and [3.5%]	LS→(0,2,2) [1.6%] and [2.6%]	LS→(1,2,0) [0.7%]
	y	(1,1,1)→(3,0,0) [29%] (0,2,0)→(0,3,0) [11%] (1,1,1)→(1,2,1) [11%] (0,0,3)→(2,1,1) [1.5%] (0,1,2)→(2,0,2) [1.9%]	(2,0,1)→(0,3,1) [3.3%]	(1,0,2)→(1,1,2) [1.4%]	(2,0,0)→(2,1,0) [1.6%] (0,2,0)→(2,1,0) [0.3%]	-	-	-	-	-	-	-	-
	z	(2,0,0)→(2,0,3) [33.5%]	(0,0,3)→(0,0,4) [6.1%]	(2,0,1)→(2,2,0) [2.8%]	(0,1,2)→(0,1,3) [2.1%] (1,0,2)→(1,0,3) [2.1%]	(1,1,1)→(1,1,2) [1.8%]	(2,0,1)→(2,0,2) [1.8%]	(0,2,1)→(0,2,2) [1.2%]	LS→(1,0,3) [19.4%] LS→(0,1,3) [16.3%]	-	-	-	-

With exception of the cases that involve the states labeled with the (1,1,1) symmetry, in the metal-to-metal electronic transitions displayed in **Table 1**, the total number of nodes change from the ground state to the excited state by an odd number. Moreover, the number of nodes in the direction of the applied field changes by either ±1 or 3 and also, in many cases, by an even number in any of the other two directions. These results are partially in agreement with the transitions selection rule of a particle in an infinite 3D well model (see derivation in **SI**). The difference is that while the infinite well model predicts allowed transitions when only one node multiplicity changes (the one in the direction of the field) by an odd number, here we obtained that a simultaneous change by an even number in any of the other two nodal multiplicities is also allowed. The reasons for this are the electron-electron interactions and the finite potential well of the real nanocluster that cause a distortion of the wave functions leading to non-zero transition dipole moment integrals. This is illustrated in **Figure 5** in an example that shows the wave functions of the states with symmetries (0,0,0) and (0,2,1) calculated from the atomistic and jellium models, and compares them with the analytical solutions of infinite 3D potential well. The product of the (0,0,0) and (0,2,1) states is plotted at the right side of the figure and the value of the integral relevant to the transition dipole moment (see **SI**) is also given for each case. Based on the infinite potential well model, transitions akin to (0,0,0)→ (0,2,1) are forbidden since the integral over the product of the two curves is 0. However, in the jellium and atomistic calculations the integral does not vanish as a consequence of the distortion of the wavefunctions beyond the box borders, indicating that this type of transitions is allowed. The derivation of the transition selection rule for a particle in a 3D infinite well is contrasted with the selection rule of more realistic models in the **SI** text. Briefly, the results of that analysis can be summarized as

follows. The selection rules for an atomistic cluster with a box-like core shape become the following: (i) such transitions are forbidden where, in the direction of the electric field, the number of nodes is changed by an even number, (ii) in addition, such transitions are forbidden, where one other number of nodes changes by an odd number. In combination, this means that for an allowed transition, exactly in one direction (of the three possibilities) the number of nodes changes by an odd number. Thus, the sum of the nodal multiplicities changes by an odd number (since odd+even+even = odd).

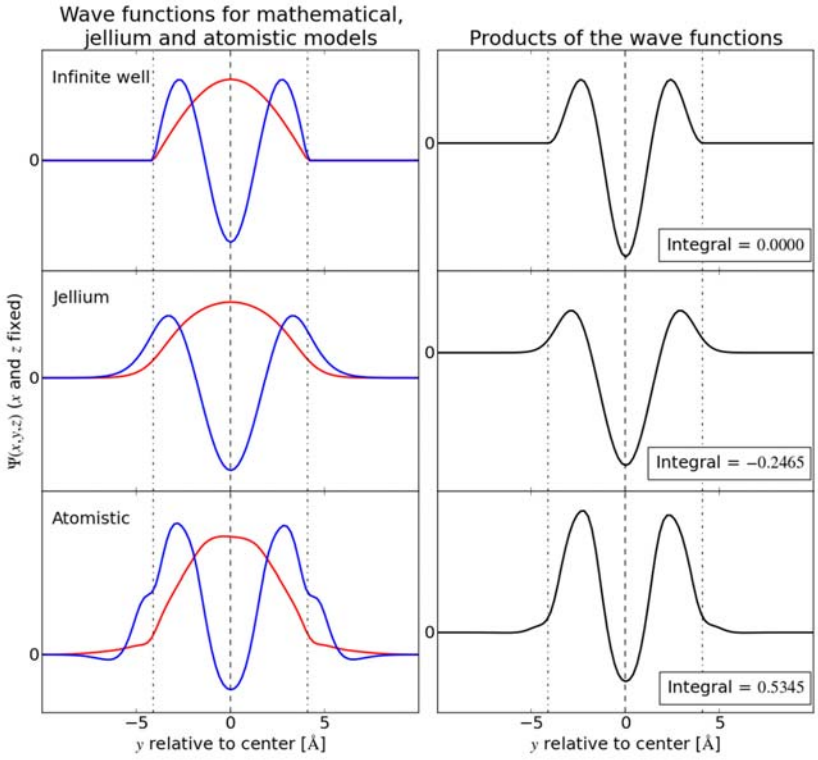

Figure 5. Wave functions for the mathematical, jellium, and atomistic models are plotted on the left for the states with symmetries (0,0,0) (in red) and (0,2,1) (in blue), and their product (in black) with the corresponding integral values are shown at the right. The curves are plotted along the *y* axis. The dashed line and dashed-dotted lines indicate the center and the borders of the box-like models.

Since each delocalized state in the atomic cluster has either an even or an odd number of nodes in each direction *x*, *y*, *z*, there are in total 8 combinations. Non-zero transitions between the states can be organized in an octant-shape "topography map", see **Figure S2** that also demonstrates again the TCM analysis of the 2.11 eV absorption peak when the occupied and empty states are classified by (odd/even ; odd/even ; odd/even) combinations.

Although in this work we focus on the particular case of the box-like $[Ag_{67}(SR)_{32}(PR_3)_8]^{3+}$ nanocluster, the strategy presented here to analyze the electronic states of an atomistic structure based on their projection onto the states of a jellium system, is a general approach that can be applied to metal nanoclusters of any core shape or aspect ratio. As an example, a few recently reported ligand-stabilized noble metal nanoclusters have polyhedral core shapes such as bi-pyramidal or Ino's decahedral shapes.[32] Nodal symmetries of the states in the metal core in such cases can be expected to match better with jellium states in a volume of a similar background shape rather than spherical superatom angular momentum states.[1]

Finally, we performed electronic calculations on two fictive box-like structures with equally good geometric stability and coordination as in the synthesized $[Ag_{67}(SPhMe_2)_{32}(PPh_3)_8]^{3+}$ nanocluster. In these two systems a block of $Ag_{21}(SH)_8$ atoms have been added or removed to/from the $[Ag_{67}(SH)_{32}(PH_3)_8]^{3+}$ model to form the compounds with chemical formulas $[Ag_{46}(SH)_{24}(PH_3)_8]^{2+}$ and $[Ag_{88}(SH)_{40}(PH_3)_8]^{2-}$, whose structures are shown in **Figure 6**. Based on the electron counting formula, the number of valence electrons in the former is 20, and 50 in the latter. For these two clusters we get HOMO-LUMO band gaps of 1.0 eV and 0.46 eV. This result may indicate even higher electronic stability compared to the known $[Ag_{67}(SPhMe_2)_{32}(PPh_3)_8]^{3+}$nanocluster whose HOMO-LUMO band gap is 0.36 eV. These results

could motivate the experimentalist to search for similar structures where the Ag_{67} extends periodically to form clusters with different aspect ratios and even longer nanorod-like structures.

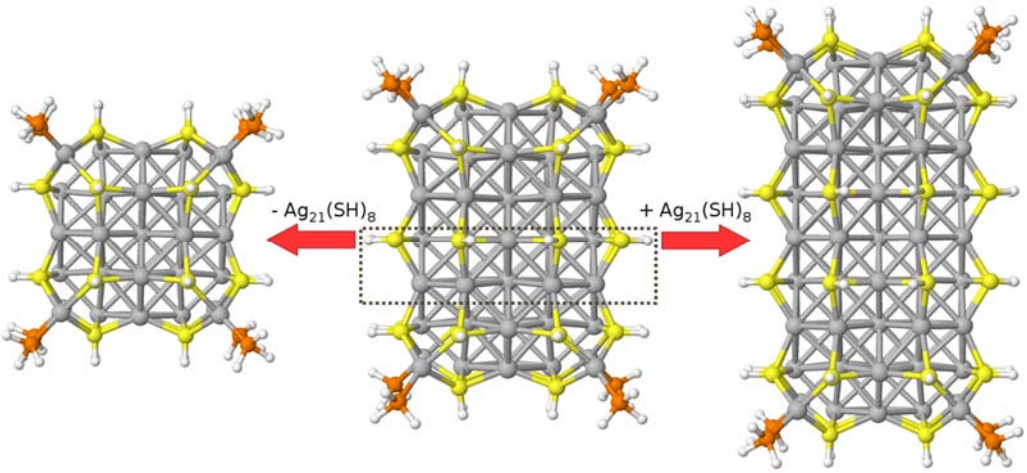

Figure 6. Side views of the (left) $[Ag_{46}(SH)_{24}(PH_3)_8]^{2+}$, (middle) $[Ag_{67}(SH)_{32}(PH_3)_8]^{3+}$, and (right) $[Ag_{88}(SH)_{40}(PH_3)_8]^{2-}$ structures. The atoms within the dashed-frame indicate the $Ag_{21}(SH)_8$ block that is added or removed to/from the $[Ag_{67}(SH)_{32}(PH_3)_8]^{3+}$ model to build the fictive nanoclusters.

CONCLUSIONS

In this work we introduced a new approach to analyze the electronic shell structure of metal nanoclusters of non-spherical shape. In this approach the symmetry of the Kohn-Sham molecular orbitals of the atomistic structure is determined based on their projection onto the "clean" states of a jellium system of similar background charge density and dimensions as in the real system. We used this strategy to determine the symmetry of the electronic states of the box-like $[Ag_{67}(SH)_{32}(PH_3)_8]^{3+}$ nanocluster and to identify the states that are involved in the most intense metal-to-metal electronic transitions. As an outcome of this work we found that in real systems consisting of multiple electrons confined in a finite potential well, the electronic transitions are

governed by a slightly different transition selection rule from the one of a particle in an infinitely deep 3D well model. Particularly we found that in nanoclusters with rectangular cuboid-like core, such as in the $[Ag_{67}(SH)_{32}(PH_3)_8]^{3+}$ system, the electronic transitions are allowed when the nodal multiplicities in the direction of the applied field changes by an odd number, as predicted by the infinite well model, but also when the other nodal multiplicities change simultaneously by an even number, leading thus to an odd number for the overall change in the total number of nodes. The deviation of this new selection rule from the one of a particle in an infinite well model demonstrates the importance of the electron-electron interactions and the finite potential of the real nanoclusters in determining allowed transitions. Furthermore, all these results demonstrate the great potential of the new approach introduced here to investigate and understand electronic shell structure, optical properties, and stability of any non-spherical nanocluster, and even to do predictions for new electronically stable nanoparticles of non-spherical structures.

ASSOCIATED CONTENT

Supporting Information: The Supporting Information is available free of charge on the ACS Publications website at DOI: .

Additional analysis of optical transitions of the Ag_{67} cluster (Figures S1, S2, and Table S1), technical discussion of overlap integrals and the selection rules for box-like systems (SI text).

AUTHOR INFORMATION

Corresponding Author

*E-mail: hannu.j.hakkinen@jyu.fi

Author Contributions

§ These authors contributed equally.

Notes

The authors declare no competing financial interest.

ACKNOWLEDGMENTS

We thank Osman Bakr for useful discussions. This work is supported by the Department of Physics at JYU (PhD scholarship for S.K.) and the Academy of Finland (project 294217 and the Academy Professorship to H.H.). The computational resources were provided by CSC-the Finnish IT Center for Science in Espoo, Finland.

REFERENCES

(1) Häkkinen, H. Electronic Shell Structures in Bare and Protected Metal Nanoclusters. *Adv. Phys. X* **2016**, *1*, 467–491.

(2) Jena, P. Beyond the Periodic Table of Elements: The Role of Superatoms. *J. Phys. Chem. Lett.* **2013**, *4*, 1432–1442.

(3) de Heer, W. A. The Physics of Simple Metal Clusters: Experimental Aspects and Simple Models. *Rev. Mod. Phys.* **1993**, *65*, 611–676.

(4) Brack, M. The Physics of Simple Metal Clusters: Self-Consistent Jellium Model and Semiclassical Approaches. *Rev. Mod. Phys.* **1993**, *65*, 677–732.

(5) Watanabe H, Inoshita, T. Superatom: A Novel Concept in Materials Science. *Optoelectronics* **1986**, *1*, 33–40.

(6) Leuchtner, R. E.; Harms, A. C.; Castleman, A. W. Thermal Metal Cluster Anion Reactions: Behavior of Aluminum Clusters with Oxygen. *J. Chem. Phys.* **1989**, *91*, 2753–2754.

(7) Leuchtner, R. E.; Harms, A. C.; Castleman, A. W. Aluminum Cluster Reactions. *J. Chem. Phys* **1991**, *94*, 1093–1101.

(8) Luo, Z.; Reber, A. C.; Jia, M.; Blades, W. H.; Khanna, S. N.; Castleman, A. W. What Determines If a Ligand Activates or Passivates a Superatom Cluster? *Chem. Sci.* **2016**, *7*, 3067–3074.

(9) *Protected Metal Clusters: From Fundamentals to Applications*, 1st Edition. Eds T. Tsukuda and H. Häkkinen, Elsevier, Amsterdam, 2015.

(10) Fernando, A.; Weerawardene, K. L. D. M.; Karimova, N. V; Aikens, C. M. Quantum Mechanical Studies of Large Metal, Metal Oxide, and Metal Chalcogenide Nanoparticles and Clusters. *Chem. Rev.* **2015**, *115*, 6112–6216.

(11) Häkkinen, H. The Gold-Sulfur Interface at the Nanoscale. *Nat. Chem.* **2012**, *4*, 443–455.

(12) Jin, R. Quantum Sized, Thiolate-Protected Gold Nanoclusters. *Nanoscale* **2010**, *2*, 343–362.

(13) Tsukuda, T. Toward an Atomic-Level Understanding of Size-Specific Properties of Protected and Stabilized Gold Clusters. *Bull. Chem. Soc. Jpn.* **2012**, *85*, 151–168.

(14) Negishi, Y. Towards the Creation of Functionalized Metal Nanoclusters and Highly Active Photocatalytic Materials UsingThiolate-Protected Magic Gold Clusters. *Bull. Chem. Soc. Jpn.* **2014**, *87*, 375–389.

(15) Sardar, R.; Funston, A. M.; Mulvaney, P.; Murray, R. W. Gold Nanoparticles: Past, Present, and Future. *Langmuir* **2009**, *25*, 13840–13851.

(16) Häkkinen, H. Atomic and Electronic Structure of Gold Clusters: Understanding Flakes, Cages and Superatoms from Simple Concepts. *Chem. Soc. Rev.* **2008**, *37*, 1847–1859.

(17) Alhilaly, M. J.; Bootharaju, M. S.; Joshi, C. P.; Besong, T. M.; Emwas, A.-H.; Juarez-Mosqueda, R.; Kaappa, S.; Malola, S.; Adil, K.; Shkurenko, A.; et al. [Ag67(SPhMe2)32(PPh3)8]3+: Synthesis, Total Structure, and Optical Properties of a Large Box-Shaped Silver Nanocluster. *J. Am. Chem. Soc.* **2016**, *138*, 14727–14732.

(18) Zeng, C.; Chen, Y.; Iida, K.; Nobusada, K.; Kirschbaum, K.; Lambright, K. J.; Jin, R. Gold Quantum Boxes: On the Periodicities and the Quantum Confinement in the Au28, Au36, Au44, and Au52 Magic Series. *J. Am. Chem. Soc.* **2016**, *138*, 3950–3953.

(19) Chen, Y.; Zeng, C.; Liu, C.; Kirschbaum, K.; Gayathri, C.; Gil, R. R.; Rosi, N. L.; Jin, R. Crystal Structure of Barrel-Shaped Chiral Au130(p-MBT)50 Nanocluster. *J. Am. Chem. Soc.* **2015**, *137*, 10076–10079.

(20) Das, A.; Li, T.; Nobusada, K.; Zeng, Q.; Rosi, N. L.; Jin, R. Total Structure and Optical Properties of a Phosphine/Thiolate-Protected Au24 Nanocluster. *J. Am. Chem. Soc.* **2012**, *134*, 20286–20289.

(21) Häkkinen, H.; Walter, M.; Grönbeck, H. Divide and Protect: Capping Gold Nanoclusters with Molecular Gold−Thiolate Rings. *J. Phys. Chem. B* **2006**, *110*, 9927–9931.

(22) Walter, M.; Akola, J.; Lopez-Acevedo, O.; Jadzinsky, P. D.; Calero, G.; Ackerson, C. J.; Whetten, R. L.; Grönbeck, H.; Häkkinen, H. A Unified View of Ligand-Protected Gold

Clusters as Superatom Complexes. *Proc. Natl. Acad. Sci. USA* **2008**, *105*, 9157–9162.

(23) Enkovaara, J.; Rostgaard, C.; Mortensen, J. J.; Chen, J.; Dułak, M.; Ferrighi, L.; Gavnholt, J.; Glinsvad, C.; Haikola, V.; Hansen, H. A.; et al. Electronic Structure Calculations with GPAW: A Real-Space Implementation of The Projector Augmented-Wave Method. *J. Phys. Condens. Matter.* **2010**, *22*, 253202-1–24.

(24) Mortensen, J. J.; Hansen, L. B.; Jacobsen, K. W. Real-Space Grid Implementation of the Projector Augmented Wave Method. *Phys. Rev. B* **2005**, *71*, 35109-1–11.

(25) Henkelman, G.; Arnaldsson, A.; Jónsson, H. A Fast and Robust Algorithm for Bader Decomposition of Charge Density. *Comput. Mater. Sci.* **2006**, *36*, 354–360.

(26) Perdew, J. P.; Burke, K.; Ernzerhof, M. Generalized Gradient Approximation Made Simple. *Phys. Rev. Lett.* **1996**, *77*, 3865–3868.

(27) Perdew, J. P.; Wang, Y. Accurate and Simple Analytic Representation of the Electron-Gas Correlation Energy. *Phys. Rev. B* **1992**, *45*, 13244–13249.

(28) M.E. Casida, C. Jamorski, F. Bohr, J. Guan, and D. R. S. Theoretical and Computational Modeling of NLO and Electronic Materials. *Recent Adv. Funct. Methods; ACS Press Washington, D.C.* **1996**, 145.

(29) Walter, M.; Häkkinen, H.; Lehtovaara, L.; Puska, M.; Enkovaara, J.; Rostgaard, C.; Mortensen, J. J. Time-Dependent Density-Functional Theory in the Projector Augmented-Wave Method. *J. Chem. Phys.* **2008**, *128*, 244101-1–10.

(30) Malola, S.; Lehtovaara, L.; Enkovaara, J.; Häkkinen, H. Birth of the Localized Surface Plasmon Resonance in Monolayer-Protected Gold Nanoclusters. *ACS Nano* **2013**, *7*,

10263–10270.

(31) Andrade, X.; Botti, S.; Marques, M. A. L.; Rubio, A. Time-Dependent Density Functional Theory Scheme for Efficient Calculations of Dynamic (Hyper)Polarizabilities. *J. Chem. Phys.* **2007**, *126*, 184106-1–8.

(32) Yang, H.; Wang, Y.; Chen, X.; Zhao, X.; Gu, L.; Huang, H.; Yan, J.; Xu, C.; Li, G.; Wu, J.; et al. Plasmonic Twinned Silver Nanoparticles With Molecular Precision. *Nat. Commun.* **2016**, *7*, 12809-1–8.

Table of Contents Graphic

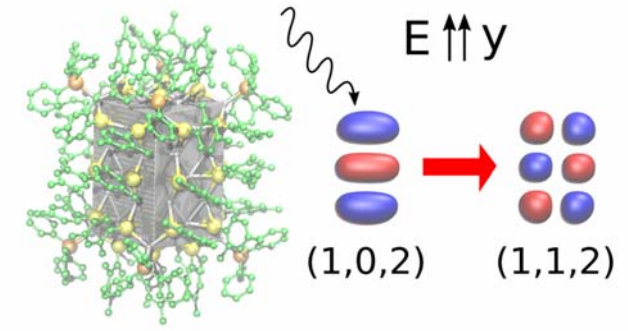

Supporting information for:

Analysis of the Electronic Structure of Non-Spherical Ligand-Protected Metal Nanoclusters: The Case of a Box-Like Ag_{67}

Rosalba Juarez-Mosqueda,[†§] *Sami Kaappa,*[†§] *Sami Malola,*[†] *Hannu Häkkinen*[*†‡]

[†]Department of Physics and [‡]Department of Chemistry, Nanoscience Center, University of Jyväskylä, FI-40014 Jyväskylä, Finland

TABLE OF CONTENTS

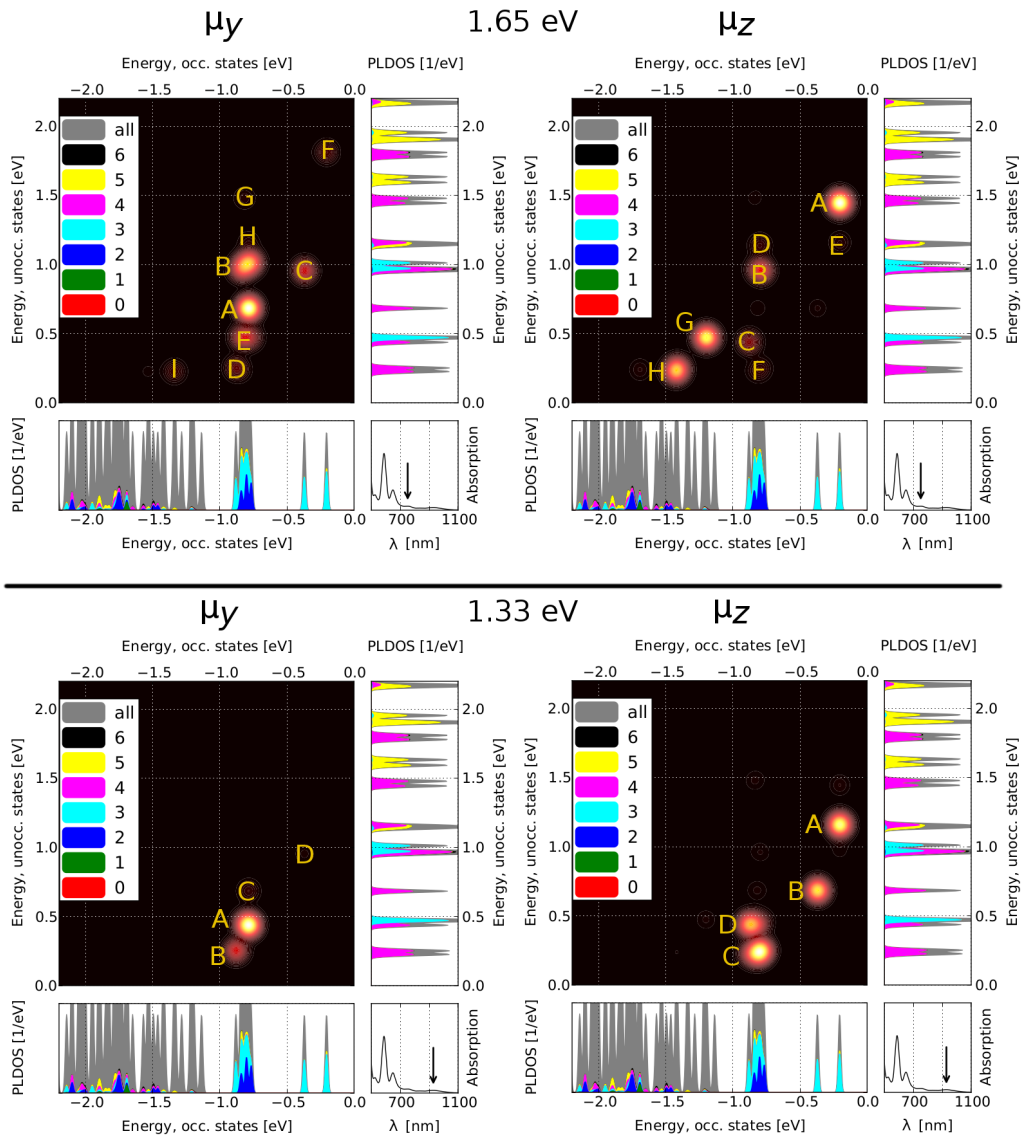

Figure S1. Transition contribution maps (TCMs) for the spectral features of the $[Ag_{67}(SH)_{32}(PH_3)_8]^{3+}$ cluster. The electronic transitions are analyzed by using photon energy of 1.65 eV (top) and 1.33 eV (bottom) and dipole moment μ directed either along the *y*- (μ_y) or *z*- (μ_z) dimension of metal core. The bright spots labeled with the letters A-I highlight the the strongest contributions. The PLDOS based on the overlap between the jellium states and the molecular orbitals of the $[Ag_{67}(SH)_{32}(PH_3)_8]^{3+}$ cluster are plotted below (occupied) and next to (unoccupied) the TCM. The colors indicate the total number of nodes. Gray shows the total density of states of the cluster. The arrow in the optical spectrum (bottom-right) points to the analyzed absorption peak.

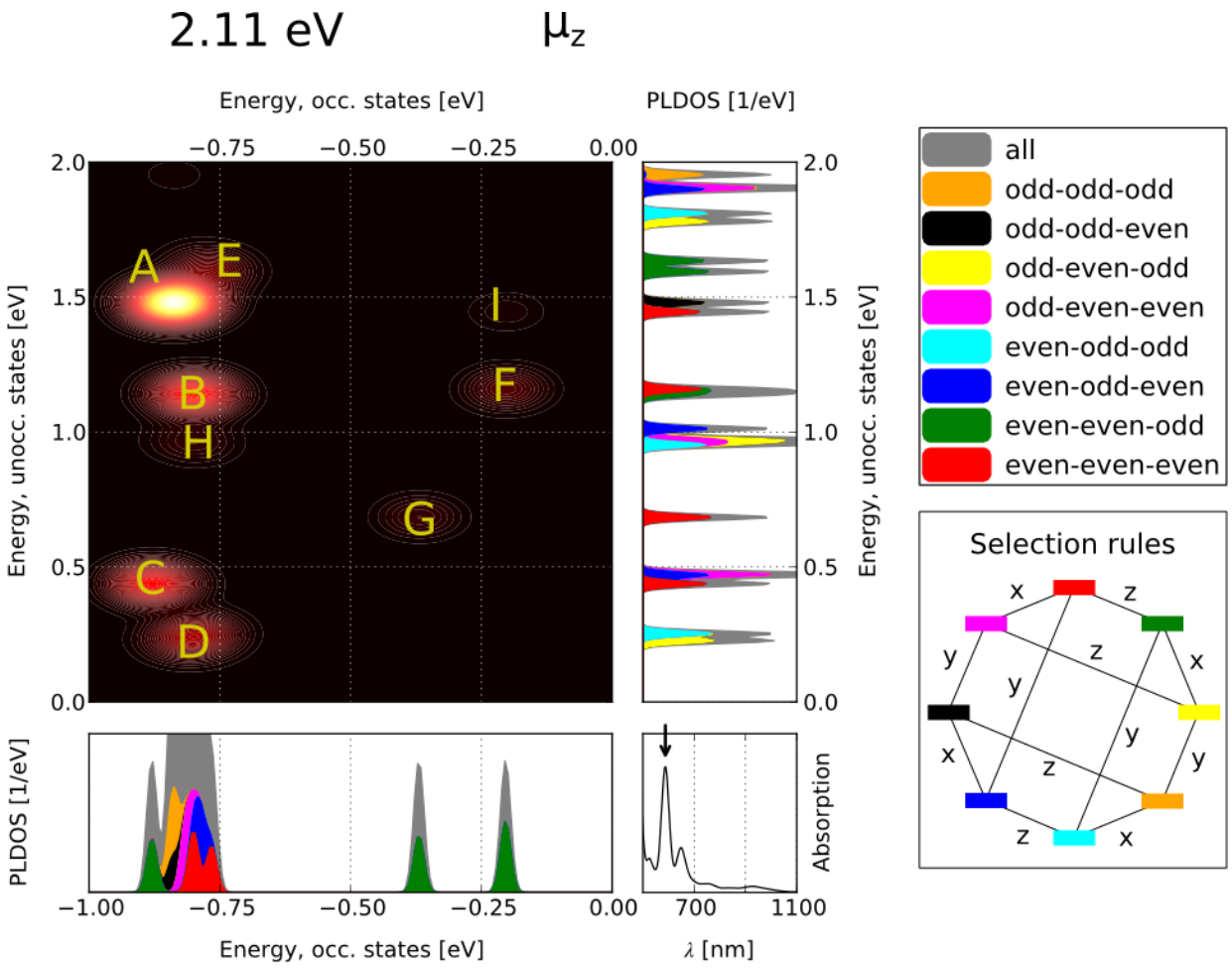

Figure S2. Transition contribution map (TCM) for 2.11eV transition with field direction along the longest edge of the Ag core, shown with different coloring of the PLDOS than the other TCM plots. The TCM corresponds to the same transitions as the upper right TCM in figure 4 (main text) with the similar labels A-I. The colors now indicate the nodal parities for each state as shown in the upper right corner. The selection rules for the nodal parities are illustrated in the lower right corner, where the lines indicate the possible transitions, for example between green and red, which denote the even-even-odd and even-even-even nodal structures, respectively. Also, the field direction in each type of allowed transition is shown, that is the direction where the parity of the nodal structure is changed. Therefore, for this TCM only the transitions with the label z are relevant. The gray area in the PLDOS, labelled as “all”, refers to the nodal multiplicities with the total number of nodes more than 6.

Table S1. Nodal multiplicities (n_x, n_y, n_z) of the Kohn-Sham molecular orbitals of the $[Ag_{67}(SH)_{32}(PH_3)_8]^{3+}$ nanocluster involved in the most intense electronic transitions. The transitions are analyzed for the absorption spectral peaks at 751 nm (1.65 eV) and 928 nm (1.33 eV) by using a laser field with the same photon energy and a dipole moment (μ) directed towards either the *y* (μ_y) or the *z* (μ_z) dimension. The letters from A-I refer to the bright spots shown in the TCMs. The values in the square brackets show the relative intensity (in percentage) of the transitions with respect to the total intensity. LS is used to indicate "ligand states".

Energy of the transition	Direction of the μ	A	B	C	D	E	F	G	H	I
1.65 eV	*y*	(0,1,2)→(0,2,2) [31.8%]	(0,2,0) →(0,3,0) [11.4%] (2,0,0)→(0,3,0) [7.7%] (1,1,1)→(1,2,1) [5.3%] (1,1,1)→(3,0,0) [2.2%]	(0,2,1)→(2,1,1) [8.8%]	(0,0,3)→(0,1,3) [3.5%]	(0,2,0)→(2,1,0) [3.3%] (2,0,0)→(2,1,0) [3.2%] (1,1,1)→(1,2,0) [3.1%]	(2,0,1)→(0,3,1) [2.9%]	(1,1,1)→(1,2,1) [2.6%] (1,0,2)→(1,1,2) [1.2%]	(0,1,2)→(2,0,2) [1.2%]	LS→(1,0,3) [1.2%]
	z	(2,0,1)→(2,2,0) [24.7%]	(0,1,2)→(2,1,1) [6.6%] (1,0,2)→(1,2,1) [1.7%]	(0,0,3)→(0,0,4) [4.2%]	(2,0,0)→(2,0,3) [1.5%]	(2,0,1)→(2,0,2) [1.0%]	(0,1,2)→(0,1,3) [0.9%] (1,0,2)→(1,0,3) [0.8%]	LS→(2,1,0) [14.8%] LS→(1,2,0) [5.0%]	LS→(1,0,3) [11.0%] LS→(0,1,3) [6.4%]	-
1.33 eV	*y*	(0,1,2)→(0,0,4) [64.6%] (1,1,1)→(1,2,0) [2.3%] (2,0,0)→(2,1,0) [1.0%] (1,1,1)→(0,0,4) [0.4%]	(0,0,3)→(0,1,3) [19%] (1,0,2)→(0,1,3) [0.2%]	(0,1,2)→(0,2,2) [4.1%]	(0,2,1)→(2,1,1) [1.6%]	-	-	-	-	-
	z	(2,0,1)→(2,0,2) [22.5%]	(0,2,1)→(0,2,2) [18.8%]	(0,1,2)→(0,1,3) [13.8%] (1,0,2)→(1,0,3) [13.3%] (0,0,3)→(1,0,3) [3.8%]	(0,0,3)→(0,0,4) [13.8%] (1,0,2)→(0,0,4) [5.1%]	-	-	-	-	-

OVERLAP INTEGRALS

The overlap integral of $\phi_i(\vec{r})$ and $\psi_j(\vec{r})$ that are the wave functions for state i from the jellium calculation and state j from the atomistic calculations, respectively, is evaluated as

$$\mathcal{O}_{ij} = \int \phi_i(\vec{r}) \cdot \psi_j(\vec{r}) \, \mathrm{d}\vec{r}. \tag{S1}$$

Because the jellium wave functions form a proper orthonormal basis, we can write the atomistic wave functions as their linear combination

$$\psi_j(\vec{r}) = \sum_a c_a \phi_a(\vec{r}) \tag{S2}$$

with c_a as the coefficients. Since this must be an orthonormal set (as the set of functions $\psi_j(\vec{r})$ is), we have the relation

$$\begin{aligned} 1 &= \int \psi_j(\vec{r}) \cdot \psi_j(\vec{r}) \, \mathrm{d}\vec{r} \\ &= \int \Big(\sum_a c_a \phi_a(\vec{r}) \Big) \cdot \Big(\sum_a c_a \phi_a(\vec{r}) \Big) \mathrm{d}\vec{r} \\ &= \sum_a c_a^2 |\phi_a|^2 \\ &= \sum_a c_a^2. \end{aligned} \tag{S3}$$

Substituting the linear combination (eq. S2) to equation S1, we notice that the overlap integrals give the coefficients for the linear combination of state j:

$$\begin{aligned} \mathcal{O}_{ij} &= \int \phi_i(\vec{r}) \cdot \sum_a c_a \phi_a(\vec{r}) \, \mathrm{d}\vec{r} \\ &= \sum_a c_a \Big(\int \phi_i(\vec{r}) \cdot \phi_a(\vec{r}) \, \mathrm{d}\vec{r} \Big) \\ &= \sum_a c_a \delta_{i,a} \\ &= c_i \end{aligned} \tag{S4}$$

For the coefficients c_i we know the property that the infinite sum of their squares equals to one (equation S3). The square of an overlap integral, $|\mathcal{O}_{ij}|^2$, thus gives the weight of a jellium state i for an atomistic state j.

SELECTION RULES FOR SYSTEMS WITH BOX-LIKE SYMMETRY

The transition dipole moment (TDM) for a transition between states i and f in the direction of the electric field $\hat{E}$ is defined as

$$\mu_{if} = \int \psi_f^*(x,y,z)(-e\hat{E}\cdot\vec{r}(x,y,z))\psi_i(x,y,z)\ \mathrm{d}x\mathrm{d}y\mathrm{d}z \tag{S5}$$

with e as the elementary charge and $\vec{r}(x,y,z) = x\hat{e}_x + y\hat{e}_y + z\hat{e}_z$ as the position vector with the origin at the center of the box. For box-shaped systems, setting the coordinate axes to lie parallel to the edges of the system lets the integral of equation S5 be evaluated in terms of symmetry of the wave functions ψ in order to manifest the selection rules for these systems.

While the wave functions for a box-shaped system must obey the same symmetry, they are either symmetric or antisymmetric with respect to the planes that cross the center of the system and whose normal vectors are parallel to the edges of the box. It also holds that the factor $\hat{E}\cdot\vec{r}(x,y,z)$ is antisymmetric with respect to the center of the box.

The trivial multiplication rules for symmetric and antisymmetric functions are the following:

- symmetric $\times$ symmetric = symmetric

- symmetric × antisymmetric = antisymmetric
- antisymmetric × antisymmetric = symmetric

The principle of the selection rules is that an integral of an antisymmetric function vanishes. Knowing the symmetries of the functions in eq. S5 as described in the last paragraph, we can determine if the total integrand becomes antisymmetric and if the integral therefore becomes 0. If the integrand is symmetric with respect to the origin, the integral can still vanish, but this only happens when the integral goes to zero both at the positive side and negative side, independently.

Let's look at a system that has analytical solutions and that best describes the real system. The wave functions for a fermion in an infinitely deep, 3-dimensional potential well are described as

$$\Psi(x,y,z) = \sqrt{\frac{8}{L_x L_y L_z}} \sin\left(\frac{n_x \pi x}{L_x}\right) \sin\left(\frac{n_y \pi y}{L_y}\right) \sin\left(\frac{n_z \pi z}{L_z}\right) \tag{S6}$$

where (n_x, n_y, n_z) is the number of maxima along (x, y, z)-axis and (L_x, L_y, L_z) is the length of the potential well along (x, y, z)-axis. Inside the box, the sinusoidal functions are symmetric wrt. the center $L/2$ if the corresponding number of maxima is odd, and antisymmetric with an even number of maxima. For simplicity, let's consider the field direction $\hat{e}_x$. Then the TDM for these analytical states becomes

$$\begin{aligned} \mu_{if} = \frac{-8e}{L_x L_y L_z} &\int_0^{L_x} \sin\left(\frac{n_{x,f}\pi x}{L_x}\right) x \sin\left(\frac{n_{x,i}\pi x}{L_x}\right) \mathrm{d}x \\ &\times \int_0^{L_y} \sin\left(\frac{n_{y,f}\pi y}{L_y}\right) \sin\left(\frac{n_{y,i}\pi y}{L_y}\right) \mathrm{d}y \\ &\times \int_0^{L_z} \sin\left(\frac{n_{z,f}\pi z}{L_z}\right) \sin\left(\frac{n_{z,i}\pi z}{L_z}\right) \mathrm{d}z \end{aligned} \tag{S7}$$

which indicates that if the number of maxima in direction $\hat{e}_x$ changes by an even number, the integral for x goes to zero and the transition is forbidden (antisymmetric integrand).

Also, due to orthogonality of the sinusoidal functions, the integrals for y and z vanish if the maximum number in $\hat{e}_y$ or $\hat{e}_z$ changes at all. Generalizing the result for any field direction, we can conclude that for functions of the form of equation S6, only such electronic transitions are allowed where one of the maximum numbers n_x, n_y and n_z is changed by an odd number.

For real systems, the rule becomes different due to the electron-electron interactions and the finite depth of the potential well. There, the wave functions are not anymore restricted to the volume of the metal core but spilled outside while losing their strict sinusoidal form. The nodal structure is preserved, however: we can label each wave function (that is delocalized in metal) with the numbers of nodes along each coordinate axis as (n_x,n_y,n_z). Note that we proceed by talking about nodes instead of maxima; the discussion ahead is valid for both cases since we are not dealing with the quantity itself but the change of the quantity in a transition, which is the same for nodes and maxima. Similar rules as for analytical solutions are valid considering antisymmetric integrands for real systems: If the node number in the direction of the field changes by an even number, the integrand becomes antisymmetric and the transition is forbidden. In addition, if the node number changes by an odd number in a direction that does not overlap with the field direction, the integrand becomes antisymmetric and the transition is forbidden.

The difference between real systems and the analytical solutions lies in transitions where one (or two) of the node numbers in a direction that is not the field direction changes by an even number. Both in real systems and in the analytical functions this results in a symmetric integrand, but in the case of the analytical solutions the integral vanishes

because of the properties of sinusoidal functions. While modelling real systems, those integrals are not necessarily zero and the corresponding transitions are not forbidden.

Therefore, the selection rules for real systems with box-like symmetry become the following:

- Such transitions are forbidden where, in the direction of the field, the number of nodes is changed by an even number
- In addition, such transitions are forbidden, where another number of nodes changes by an odd number.

To generalize, in an allowed transition exactly one node number (of the three numbers along the edges of the box-like system) changes by an odd number. It follows that in an allowed transition the total number of nodes changes by an odd number (odd + even + even = odd).